5-1-2018

A Characterization of {10T̄2} and {10T̄1} Microevolution in Magnesium under Uniaxial Tension

William Donald Russell

A characterization of $\{10\bar{1}2\}$ and $\{10\bar{1}1\}$ microevolution in magnesium under uniaxial tension

By

William Donald Russell

A Thesis
Submitted to the Faculty of
Mississippi State University
in Partial Fulfillment of the Requirements
for the Degree of Master of Science
in Mechanical Engineering
in the Department of Mechanical Engineering

Mississippi State, Mississippi

August 2018

A characterization of $\{10\bar{1}2\}$ and $\{10\bar{1}1\}$ microevolution in magnesium under uniaxial tension

By

William Donald Russell

Approved:

_____

Haitham El Kadiri
(Major Professor)

_____

Andrew L. Oppedal
(Committee Member)

_____

Christopher Barrett
(Committee Member)

_____

Yucheng Liu
(Graduate Coordinator)

_____

Jason Keith
Dean of
Bagley College of Engineering

Name: William Donald Russell

Date of Degree: August 10, 2018

Institution: Mississippi State University

Major Field: Mechanical Engineering

Major Professor: Dr. Haitham El Kadiri

Title of Study: A characterization of $\{10\bar{1}2\}$ and $\{10\bar{1}1\}$ microevolution in magnesium under uniaxial tension

Pages in Study 39

Candidate for Degree of Master of Science

Hexagonal close packed (hcp) crystal structures, such as magnesium and titanium, provide formidable strength in relation to density. Current interests in reducing CO_2 emissions, hold magnesium as a contender to lightweight passenger vehicles. Although significant decreases in mass could be achieved through magnesium, poor formability and energy absorption capacity limit the possibility for cost-effective production. This Master's thesis aims to observe the microstructure and micro texture evolution induced by twinning using interrupted electron backscattered diffraction (EBSD) characterization in order to determine potential mechanisms causing early failure of magnesium alloys. This study revealed $\{10\bar{1}1\}$ contraction twins at stress levels contrary to the basic hypothesis of the Schmid effect revealing the importance of non-Schmid effects in damage. Furthermore, it was observed that crack nucleation occurs in magnesium alloys, due mainly to interaction between twins and microstructure defects and form inside contraction twins, causing cleavage-like terraces in the fracture surface.

DEDICATION

I would like to dedicate this work to my late grandfather Dr. Donald Reid Russell for his support throughout my life. He is surely missed, and I will continue to live my life upholding the values he has instilled in my heart.

ACKNOWLEDGEMENTS

I would like to thank all who have influenced my research and myself, specifically Dr. Haitham El Kadiri, Dr. Andrew Oppedal and Dr. Christopher Barrett. I would also like to show my gratitude for the faculty and staff of the Center for Advanced Vehicular Systems and Mississippi State University for their assistance in educating and contribution to the methods described in this thesis. I would also like to thank Mississippi State University and the U.S. Army Engineer Research and Development Center for funding this research.

TABLE OF CONTENTS

DEDICATION ii

ACKNOWLEDGEMENTS iii

LIST OF TABLES v

LIST OF FIGURES vi

CHAPTER

I. INTRODUCTION 1

II. METHODS AND MATERIALS 7

2.1 Experimental Procedure 7
2.2 Areas of Interest 10

III. RESULTS AND DISCUSSION 12

3.1 Interruptive EBSD Characterization in AOI 1 12
3.2 The Characterization of Contraction Twinning in AOI 2 19
3.3 Twin-interactions Induced Cracks 27

IV. CONCLUSIONS 33

REFERENCES 35

LIST OF TABLES

3.1 Values of Resolved Shear Stress and Schmid factors determined by a [0001] loading with applied stress at yield of ET-Tension in Figure 2.2 13

3.2 Schmid factors of the three distinct {1012} pairs with [101 30] loading 14

3.3 Values of Resolved Shear Stress and Schmid factors determined by a [2110] loading with applied stress at 2% Strain of ET-Tension in Figure 2.2 24

LIST OF FIGURES

1.1 A schematic illustrating crack nucleation at the intersection of two twins, by Reed-Hill [5] 3

1.2 Twin-GB interaction-induced regions of high stress (dark blue regions) leading to GB crack initiation in Mo according to MD simulations by Zhang et al. [10]. 4

2.1 {0001} and {1010} pole figures obtained from neutron diffraction analysis showing a double fiber texture of AM30 magnesium alloy. The extrusion direction (ED) is along the z-axis making the extrusion transverse direction (ET) along the x-axis and the extrusion normal direction (EN) along the y-axis. The regions shown in green and blue indicate high concentrations of [2110] and [1010] oriented grains parallel with the extrusion direction respectively. Scale shows multiples of random distribution [21] 8

2.2 Stress-Strain relationship of AM30 alloy in extrusion and extrusion transverse directions. A sigmoidal curve for tension along the extrusion transverse (ET) direction indicates high strain hardening which is characteristic of profuse tension twinning,. while tension along the extrusion (ED) direction alludes to deformation due to slip with minimal twinning [21]. 9

2.3 The magnesium AM30 crush rail is an extrudate component used in automotive shock absorption structure. This extrusion allows plane-strain conditions on the flat sections that promote a desirable double-fiber texture for studying twins as it promotes nucleation of multiple twin modes and variants in tension within neighboring grains. 10

2.4 (a) Inverse Pole Figure map generated by Electron Backscatter Diffraction (EBSD) analysis using the FEG-SEM, showing initial state of microstructure before deformation. (b) The highlighted partitions of the areas of interest (AOI 1 and AOI 2) with discrete unit crystal orientations are the focus of the study. 11

3.1 (a) Inverse pole figure maps at various incremental strains ranging from 0% to 5%. The tensile load is applied horizontally with respect of the image. The six variants of the {1012} tensile twins nucleate and propagate in the parent grains resulting in a fully reoriented grain by 5% strain. (b) Contraction twin formation from the (1102) and (1102) twins' interaction with the GB. 15

3.2 Twin variant selection in AOI 1. (a) The orientation map of the three evident twin pairs highlighted in green yellow red. (b) By mapping the grain boundary occupancy of twins at 1% strain (just after nucleation), the perimeter fraction of twinning can be determined. The perimeter fraction shows a clear dominance of (1012) twinning with evident dominate variants within the green and yellow pairs, i.e. (0112) and (1102) respectively. (c) The proposed variant pair twin planes are shown within parent orientation with their respective highlighted colors. 17

3.3 (a) Evolution of twin variant area fraction with strain for the three distinct pairs of the {1012} system in AOI 1. (b) (0001) pole figures showing the nucleation of three dominate twin variants forming at 1% strain then growing in intensity as the parent orientation diminishes. 18

3.4 (a) Inverse pole maps revealing lattice reorientation due to profuse nucleation of {1011} contraction twinning and slip as deformation proceeds from 0% to 5%. Although pyramidal slip ⟨c+a⟩ has a relatively higher SF, there is profuse nucleation of contraction twins. (b) The misorientation data of the twins indicates the presence of contraction twins as early as 2% of strain with unit crystal orientation of both twins. 22

3.5 Characterization of {1011} contraction twins at (a) 4% strain revealing continuous nucleation of new twin variants. The twins were individually selected to be partitioned from the parent grain. The texture of the partitioned twins is shown in part (b). Double twins are found among the partitioned twins. The idealized texture of {1011} contraction twins is shown in part (c). Not all twin variants are present, but they are representatives of each twin pair are. The contraction twin variants are characterized by their respective color pair highlighted in the parent grain (a), PF (b, c), and crystal lattice (d). 23

3.6 Characterization of double twinning at low stresses. The twin of interest is fully formed by 3% strain and does not show signs of double twinning. By 4% strain, the twin of interest begins to double twin at the middle. Misorientation analysis between the double twin and the contraction twin is compared to confirm the presence of contraction and double twins. 26

3.7 Comparison of the stress states experienced by (a) In Plane Compression and (b) [2110] Tension. The representation of [2110] Tension is simplified to a two-dimensional planer stress representing the plane of maximum compression in an attempt to visualize the complexity of the stress state experienced by contraction of the c-axis due to Poisson Effects. 26

3.8 Micrographs depicting Slip-Twin interactions' involvement in crack nucleation [33]....27

3.9 Twin-GB interactions lead to crack nucleation (a) due to a lack of strain accommodation. (b) Proper accommodation of strain is found at the surface where GB emerges through "kinking." However, a crack is formed at the GB from interactions with another twin. Cracks are also noted from twin-twin interactions [33]. 29

3.10 Micrographs of {1012} Twin-Twin interactions and their involvement in crack nucleation [33]. 29

3.11 Micrographs of evident contraction twins near massive crack nucleation [33]....30

3.12 Large crack formation due to contraction twin interactions. The contraction twins are found to have a misorientation of 56° [33]. 31

3.13 Micrograph shows evidence of dual phase fracture. Cleavage and stepped terraces formed from twin interactions caused brittle failure while the tormented regions induced ductile failure [33]....31

4.1 Multiscale effects driving plasticity and damage in magnesium....34

CHAPTER I

INTRODUCTION

The reduction of greenhouse gases (GHG) and reduced dependence on hydrocarbon-based fuels is a key priority worldwide. The United States, Canada, China and the Euro-zone have engaged, in a first stage plan to reduce the mass of CO_2 emitted by passenger vehicles a full 30-50% below current standards by the year 2020 (targets: 95g/km for EU and China; 110g/km for the USA and Canada). Such tremendous improvements will require extensive vehicle mass reduction through the use of lightweight materials allowing for (1) a net fuel economy improvement in combustion engine and (2) an increase in the range of electric vehicles. In addition, all material developments must maintain or improve crash worthiness of current vehicles.

Two of the most attractive metals that have potential to satisfy these conflicting demands, magnesium (Mg) and titanium (Ti) alloys, exhibit a hexagonal close-packed (hcp) crystal structure at room temperature. While Ti is too expensive for automotive applications, current structural applications of hcp Mg alloys are limited to castings due to difficulties associated with forming wrought alloys. In order to increase applications of these lightweight materials in response to the critical needs within the transportation sector, improvement in both their formability and ability to absorb energy during a crash is required.

The plastic anisotropy of the hexagonal lattice is widely understood as the source of the present limitations associated with hcp metals. The dislocations that accommodate plasticity in hcp crystals generally have Burgers vectors within the basal plane. Thus, these materials suffer from an inability to deform easily along the crystal c-axis by slip, requiring deformation twinning-based mechanism of strain accommodation. Deformation twinning has long been known to alleviate the requirement to satisfy the von Mises criterion for polycrystalline plasticity that requires five independent dislocation slip modes. However, deformation twinning-based plasticity can be a "double-edged sword." It has been demonstrated through literature that twinning is associated with fracture initiation, and there are a number of micro-mechanism hypotheses to explain these phenomena which are based on the strain incompatibility that arises when a twin meets a certain microstructure obstacle (e.g. grain boundary or another twin), or when dislocations meet a twin interface.

In fact, when a deformation twin is nucleated at a grain boundary (GB), propagates across a grain, and reaches the opposite GB, the plastic shear brought about by this twin can be either accommodated by surface kinking, slip or twinning at the GBs [1]. This process is known as accommodation effects.

Accommodation effects by slip and kinking are of considerable importance to understand strain incompatibility induced by twinning. While kinking arises in the case where the twin emerges at the free surface, e.g. single crystals, accommodation in polycrystals are mainly facilitated by means of slip or another twin (interaction twins). If the GB has a low misorientation allowing the adjacent grain to have a high local Schmid factor for the same twinning variant/mode, twinning can be readily activated in the

adjacent grain. This is a particular case for sharp, basal textures where twins could be observed traversing an entire sample from one edge to another edge. However, if the GB has a sufficiently high misorientation leading to a low local Schmid factor for twinning in the adjacent grain, which could arise in weak textures, slip is necessary or otherwise a crack may nucleate to drive fracture [2–4]. Crack nucleation at the termination of an incident twin meeting an obstacle twin has been actually reported as early as 1868 by Rose [5] (Figure 1.1), and later by Sleeswyk [6–8] to explain ductile-brittle fraction transition in bcc iron through a complex emissary dislocation proposed mechanism. Twin-accommodation effects at GBs and twin boundary (TB)s bear critical implications for damage initiation in hcp structures [9]. Recently, Zhang et al. [10] showed via MD simulations the opening of cracks in bcc Molybdenum at a GB into which a deformation twin impinges (Figure 1.2).

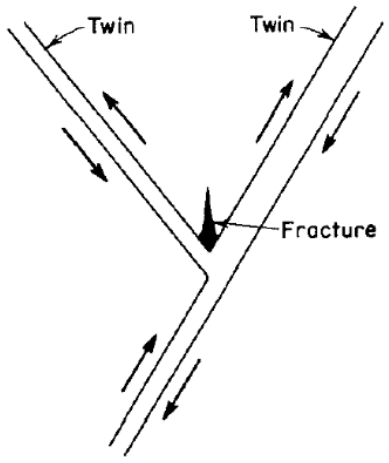

Figure 1.1 A schematic illustrating crack nucleation at the intersection of two twins, by Reed-Hill [5]

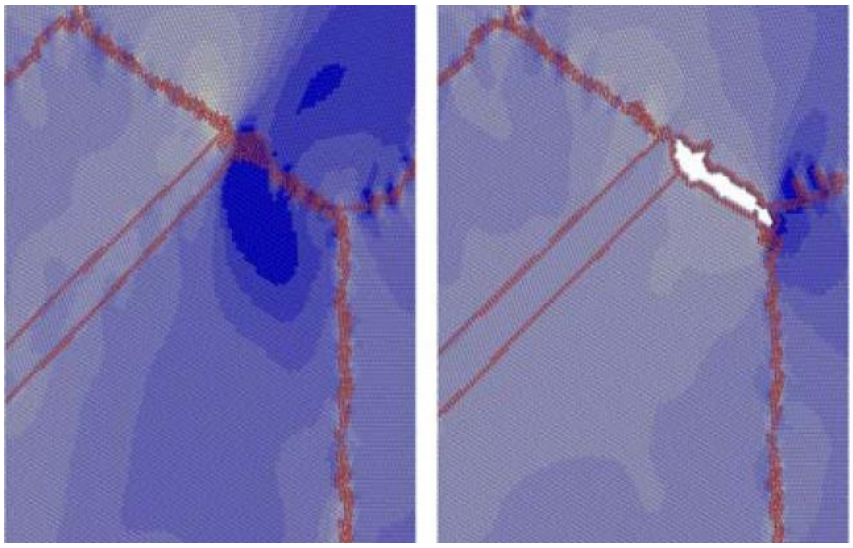

Figure 1.2 Twin-GB interaction-induced regions of high stress (dark blue regions) leading to GB crack initiation in Mo according to MD simulations by Zhang et al. [10].

In general, even for largely unconstrained single crystals (SC), the shape change of twinning may be partly accommodated by kinking and/or slip [11–13]. Holden [11], observed that non-basal slip should trigger in most cases to relax any strain incompatibility in pure hcp metals. However, in the case of stronger hcp alloys such non-basal slip systems tend to be much harder to activate than the basal slip counterparts, which would promote hot stress spots and local fracture initiation. This could perhaps explain why twinning is not as deleterious to ductility in fcc as hcp metals, considering that the critical resolved shear stresses (CRSSs) remain the same for all active slip dislocations (practically one slip mode). Although the role of twin-accommodation slip in plasticity was invoked and emphasized since the nineteen fifties and sixties, current crystal plasticity, and thus, continuum mechanics models still largely ignore it. The difficulty of activating slip might be exacerbated by inter-granular particles and solutes, so cracks may readily open at the termination of twin in alloys as suggested by Rémy

[14,15]. Finally, all these events are compounded with classical effects of slip on strain incompatibility and thus localization. GBs are lattice orientation discontinuities over which strain incompatibility arises. Local phenomena are more pronounced in triple junctions and quadruple points where deformation is more than two grains influence the effective lattice rotation.

From the macroscopic standpoint, if one assumes that twinning is responsible for the limited ductility of magnesium, it is not yet clear why ductility is still unacceptable for fibers loaded under a loading orientation where $\{10\bar{1}2\}$ tension twinning activity is minimized. For instance, when a basal texture is pulled normal to the fiber axis, prismatic $\langle a \rangle$ and pyramidal $\langle c + a \rangle$ slip should be the dominant deformation mechanisms and though an improvement in total elongation is obtained, compared to the case of profuse twinning having a sigmoidal stress-strain curve, necking does not take place and fracture occurs in a brittle-like fashion. One may argue that locally, twinning occurs as a result of slip-induced lattice rotations. However, the amount of rotation remains largely incapable to bring a favorable orientation of $\{10\bar{1}2\}$ twinning. There are reports of $\{10\bar{1}1\}$ [16,17] (also $\{10\bar{1}3\}$ and $\{10\bar{2}4\}$) formation in magnesium alloys that could be very deleterious to ductility [18,19]. Most of these reports suggest that the CRSS is so high that they would only appear inside $\{10\bar{1}2\}$ twins during the saturation stage of stress after the rapid hardening correlated with profuse twinning [17]. In crystal plasticity simulations of pure magnesium, Oppedal et al. [20] used a CRSS value of 181 MPa for $\{10\bar{1}1\}$ twinning compared to 11 MPa for basal $\langle a \rangle$, 15 MPa for $\{10\bar{1}2\}$ twinning, 30 MPa for prismatic $\langle a \rangle$, and 50 MPa for the very hard pyramidal $\langle c + a \rangle$. In general, $\{10\bar{1}1\}$ twinning has a high Schmid factor in this loading orientation but because of its high CRSS, it is not

expected to form at the relatively low saturation stress levels attained during tension normal to the basal fiber.

In an effort to bring experimental evidence and elucidate the dominant damage mechanisms involving twinning in hcp metals, we performed interrupted electron back-scattered diffraction characterization on the flats formed in a plane-strain environment found in an extruded AM30 magnesium alloy crush rail showing a double-fiber texture, which allows both profuse and no twinning in neighboring grains under the same uniaxial tension. On one hand, this would allow a closer study of damage caused by various twin variant interactions, as these twins grow in favorably oriented grains belonging to the ET||(0001) (resp. EN||(0001), as well as parsing their effect on texture evolution within each grain. On the other hand, these grains might be surrounded with grains prohibiting twinning which would provide the opportunity to study the effect of twin-accommodation mechanisms on damage.

CHAPTER II

METHODS AND MATERIALS

2.1 Experimental Procedure

Magnesium alloy AM30 with a chemical composition (wt. %) of 2.83Al, 0.386Mn, 0.0037Zn, 0.03Fe, <0.0015Ni, <0.0005Cu, balance Mg was the material of this study. Extrusion of this AM30 alloy was performed by Timminco. The process began with pre-extrusion to bring down the diameter of the cast billet from a 18 inch to 9 inch diameter cylinder through a 4200-ton press which ran up to a maximum pressure of 3200 psi and then pushed the 9 inch billet through the final die at 2400 psi. The entrance and the exit temperature were around 440 C and 540 C, respectively. The ram speed for the extrusion was about 3.1 in/min, while the extrusion speed was about 9 ft/min. The extrusion ratio was 35.26/1. Lastly, the billet was extruded into the final shape, which corresponded to a hollow tube in "double-hat" like shape, known as a crush rail (Figure 2.3). This crash rail showed a texture that has a strong basal pole aligned with the in-plane direction of the sheet normal to the extrusion direction (extrusion traverse, or ET), and a weak basal texture component in the normal direction of the sheet (EN) (Figure 2.1). As such, under tension along ET (resp. EN), several grains belonging to the ET||(0001) fiber (resp. EN||(0001) fiber), would be subject to the formation of all six $\{10\bar{1}2\}$ twin variants contributing to their very large Schmid factor (0.499). While grains belonging to the EN||(0001) (resp. ET||(0001) fiber) fiber will experience favorable

conditions for slip mechanisms to take place exclusively and perhaps $\{10\bar{1}1\}$ twins if enough stress is attained macroscopically. Specimens machined in extrusion (ED) and extrusion transverse directions (ET) were polished using 4000 grit silicon carbide paper and then electrochemically polished with C1 electrolyte for 20 seconds to pristine finish. Through interrupted electron backscatter diffraction (EBSD) analysis on specific regions, the evolution of deformation and damage was studied. Figure 2.2 shows stress-strain curves obtained at 0.001/s strain rate when the specimens were taken to full fracture, which delineate traditional anisotropy of magnesium that is associated with basal and rod fiber textures. Under ED direction compression loading, $\{10\bar{1}2\}$ twinning is nearly non-existent yielding to a parabolic stress-strain behavior, while under ET all of the grains belonging to the strong ET||(0001) fiber experience profuse $\{10\bar{1}2\}$ twinning eventuating to a sigmoidal curve with very rapid hardening.

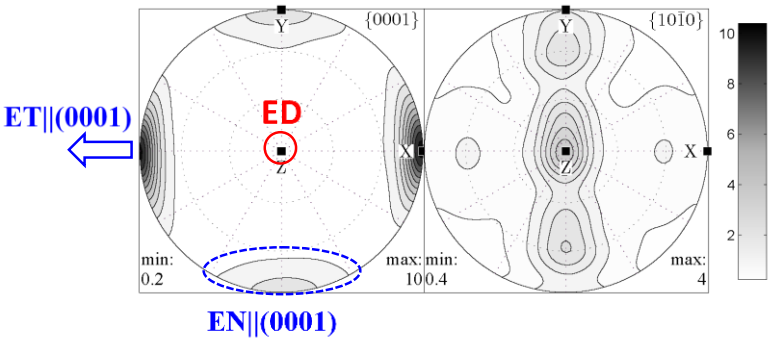

Figure 2.1 {0001} and $\{10\bar{1}0\}$ pole figures obtained from neutron diffraction analysis showing a double fiber texture of AM30 magnesium alloy. The extrusion direction (ED) is along the z-axis making the extrusion transverse direction (ET) along the x-axis and the extrusion normal direction (EN) along the y-axis. The regions shown in green and blue indicate high concentrations of $[2\bar{1}\bar{1}0]$ and $[10\bar{1}0]$ oriented grains parallel with the extrusion direction respectively. Scale shows multiples of random distribution [21].

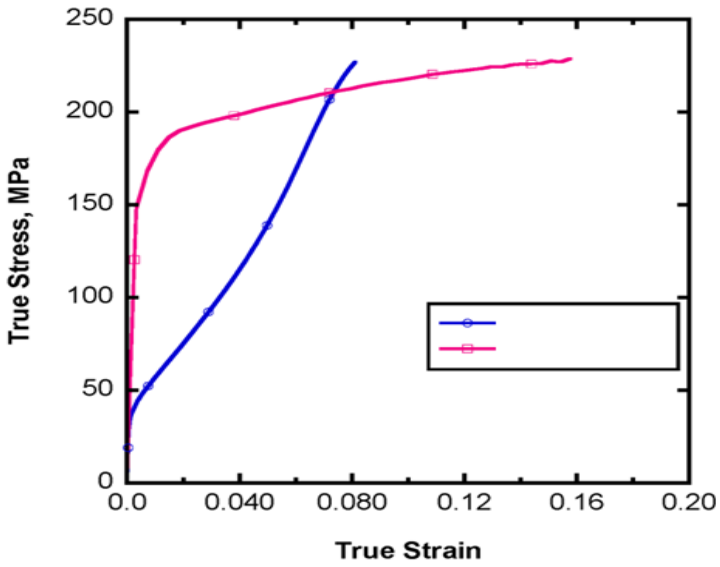

Figure 2.2 Stress-Strain relationship of AM30 alloy in extrusion and extrusion transverse directions. A sigmoidal curve for tension along the extrusion transverse (ET) direction indicates high strain hardening which is characteristic of profuse tension twinning,. while tension along the extrusion (ED) direction alludes to deformation due to slip with minimal twinning [21].

The interrupted EBSD characterization and collection were performed with a Zeiss Supra 40 field emission scanning electron microscope (FEG-SEM) equipped with an orientation image microscopy (OIM EDAX TSL) at a step size of 100 nm on large regions of the samples. These EBSD analyses were completed using the commercially available TSL OIM Analysis software from EDAX. Neutron diffraction texture analysis was conducted with the HIPPO neutron time-of-flight diffractometer at LANSCE [22]. The pole figure data was exported from MAUD [23] and imported into MTEX [24] for further ODF (orientation distribution function) analysis. Intermittent monotonic tension tests were performed using an Instron 8856 at a quasi-static strain rate ($0.001s^{-1}$). After failure, fractographic analysis were conducted using the FEG-SEM to determine the overall causation of failure.

2.2 Areas of Interest

Most of observation were conducted on sections normal to ET. The specimen was taken from the crash rail in such a way to avoid irregular texture created by welding in the extrusion process. We identified two contiguous areas of interest (AOI) shown in the initial microstructure of Figure 2.4 which are expected to show very different levels of twinning (Region AOI 1 and Region AOI 2). AOI 1 is composed of three primary grains all of which prescribe to the $[11\bar{2}0]$ orientation with the c-axis along the line of tension, and as such favorable for $\{10\bar{1}2\}$ twinning (belonging to ET||(0001) fiber). AOI 2 is also composed of the three primary grains showing a [0002] basal texture meaning the c-axis is perpendicular to the loading direction (belonging to EN||(0001) fiber). This region should experience a dominance of slip deformation mechanisms, specifically basal ⟨a⟩, prismatic ⟨a⟩, and pyramidal ⟨c+a⟩ [21].

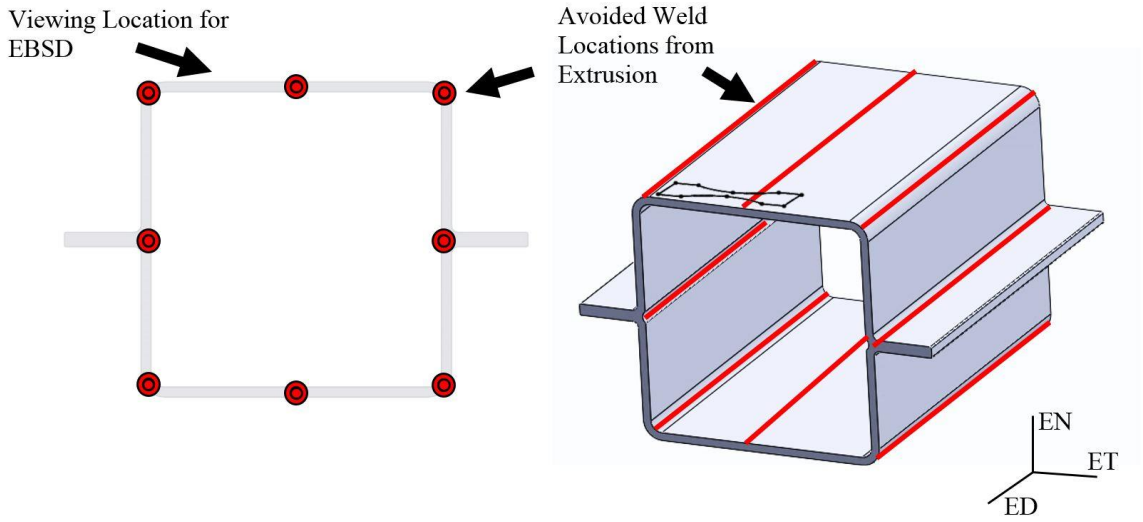

Figure 2.3 The magnesium AM30 crush rail is an extrudate component used in automotive shock absorption structure. This extrusion allows plane-strain conditions on the flat sections that promote a desirable double-fiber texture

for studying twins as it promotes nucleation of multiple twin modes and variants in tension within neighboring grains.

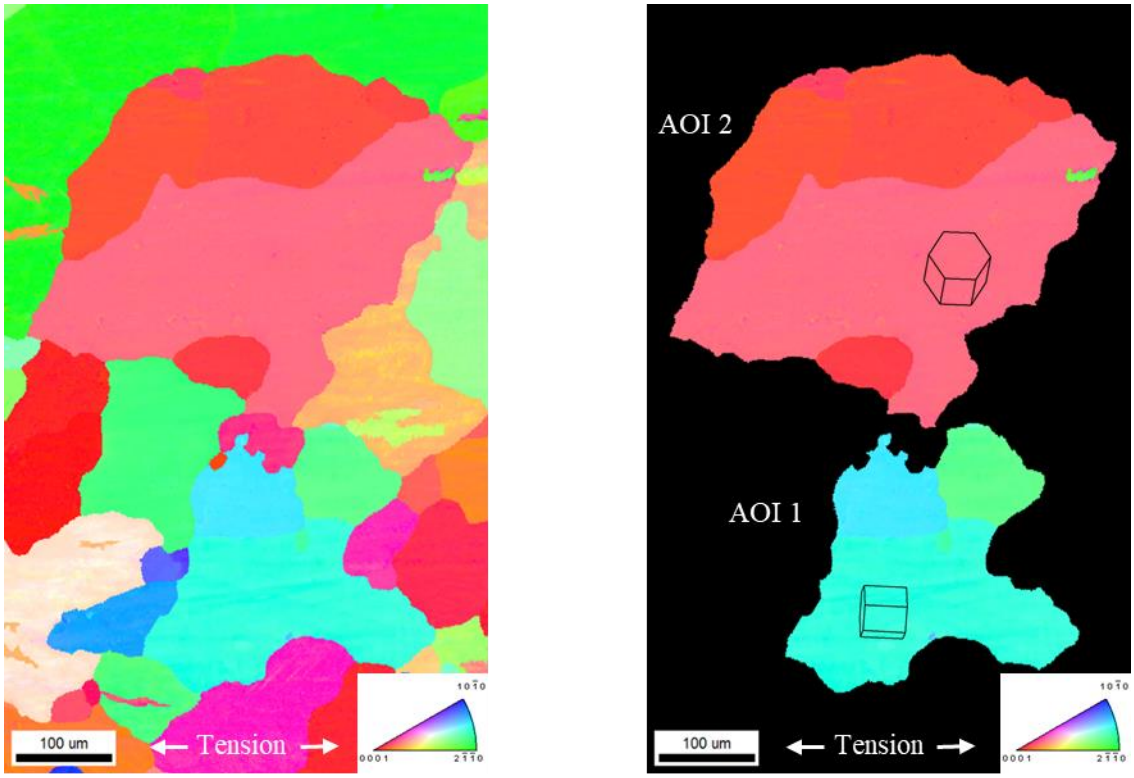

[A] [B]

Figure 2.4 (a) Inverse Pole Figure map generated by Electron Backscatter Diffraction (EBSD) analysis using the FEG-SEM, showing initial state of microstructure before deformation. (b) The highlighted partitions of the areas of interest (AOI 1 and AOI 2) with discrete unit crystal orientations are the focus of the study.

CHAPTER III

RESULTS AND DISCUSSION

3.1 Interruptive EBSD Characterization in AOI 1

Figure 3.1 shows that AOI 1 readily experiences $\{10\bar{1}2\}$ tensile twinning caused by the extension of the c-axis. Resolved Shear Stress (RSS) is commonly used to determine the likelihood of elevation of stress through slip or twins. The RSS is dependent on the Schmid factor (SF), $0 \leq SF < 0.5$, of slip or twin plane of interest and the applied stress (σ_{app}) of the material [25] (Table 3.1 describes the RSS of possible slip and twin systems). With all variants of $\{10\bar{1}2\}$ tensile twins having near maximum SF values, all variants are expected to be present in the EBSD micro textures.

Table 3.1 Values of Resolved Shear Stress and Schmid factors determined by a [0001] loading with applied stress at yield of ET-Tension in Figure 2.2

	Slip or Twin Plane (h k (i) l) [u v (t) w]	Schmid Factor SF	Resolved Shear Stress RSS (MPa)
Tension Twin Variants	$(\bar{1}\ 0\ 1\ 2)\ [1\ 0\ \bar{1}\ 1]$	0.499	19.96
	$(1\ 0\ \bar{1}\ 2)\ [\bar{1}\ 0\ 1\ 1]$	0.499	19.96
	$(0\ \bar{1}\ 1\ 2)\ [0\ 1\ \bar{1}\ 1]$	0.499	19.96
	$(0\ 1\ \bar{1}\ 2)\ [0\ \bar{1}\ 1\ 1]$	0.499	19.96
	$(1\ \bar{1}\ 0\ 2)\ [\bar{1}\ 1\ 0\ 1]$	0.499	19.96
	$(\bar{1}\ 1\ 0\ 2)\ [1\ \bar{1}\ 0\ 1]$	0.499	19.96
Slip Systems	Basal $\langle a \rangle$	0	-
	Pyramidal $\langle a \rangle$	0	-
	Pyramidal $\langle c + a \rangle$	0.401	16.04

When determining the twin variants, multiple factors are checked to confirm a twin variant. The simplest of these is boundary misorientation of twin and parent. In the case of all twins present, the misorientation is found to be 86° (± 8°). We also know that the c-axis of the parent grain is in line with the loading direction allowing extension of the c-axis, which promotes tensile twins. With evidence of confirmed tensile twins, we specified the Miller-Bravais indices of each twin based on a reference frame choice. The data from the EBSD analysis is used to create an orientation map, which highlights similar areas of lattice orientation based on the angle of the c-axis. This map is shown in Figure 3.2 alongside the twin planes of the $\{10\bar{1}2\}$ system. The six twin variants found in the $\{10\bar{1}2\}$ system are made up of three distinct twin pairs and are highlighted as such in Figure 3.2. Each orientation of the present twins was used to calculate the SF of each

twin plane. The average SF for each twin pair under a non-idealized $[10\bar{1}\ 30]$ loading is shown in Table 3.2.

Table 3.2 Schmid factors of the three distinct $\{10\bar{1}2\}$ pairs with $[10\bar{1}\ 30]$ loading

Tensile Twin Pairs	$(0\bar{1}12)$	$(\bar{1}102)$	$(\bar{1}012)$
Schmid Factor (SF)	0.219	0.478	0.245

Incremental ET tensile tests of the AM30 with interrupted EBSD scans show the nucleation and progression of twins in AOI 1 (Figure 3.1). At 0% strain, very small $\{10\bar{1}2\}$ tensile twins were observed in the top right grain of AOI 1. The twins likely nucleated after grinding and polishing and their orientations are found to have a Schmid factor of m=0.43. The stress strain relationship is commonly categorized by three regimes. The first regime represents the elastic portion of the response while the second encompasses the plastic strain leading to an inflection point in this case, the transition from twin nucleation dominated to twin growth dominated strain accommodation and the final regime represents the continuation of plastic deformation until failure. Within Regime I of the strain relationship, twins readily nucleate from relatively high misorientation GBs before 1% of strain was reached. Although six tensile twin variants are present, the presence of a dominant variant of each distinct pair is conspicuous. This was associated by the ability of nucleating at all possible sites while the recessive variant nucleates from other twin boundaries. The dominant variant of each pair is easily distinguished in the pole figures of Figure 3.3b.

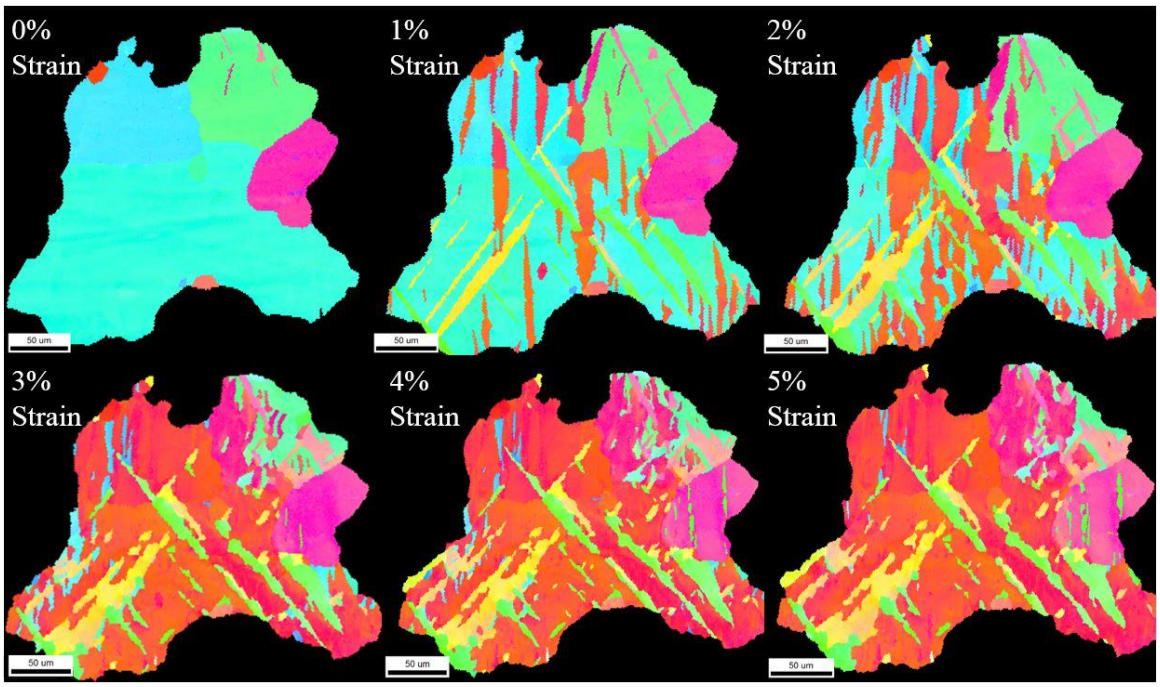

[A]

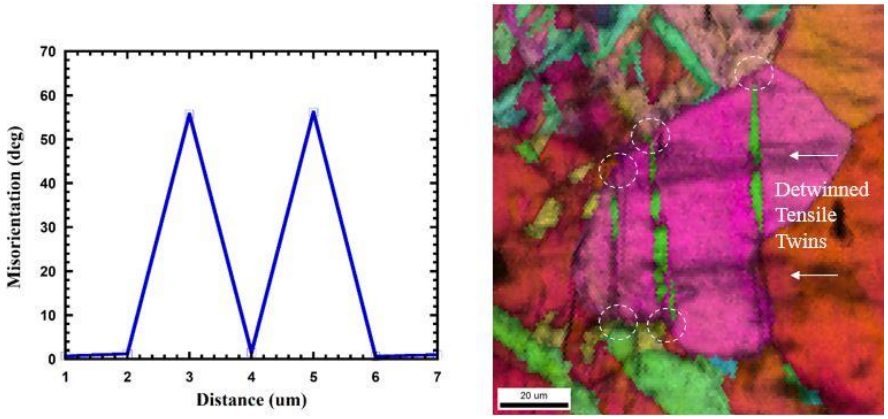

[B]

Figure 3.1 (a) Inverse pole figure maps at various incremental strains ranging from 0% to 5%. The tensile load is applied horizontally with respect of the image. The six variants of the $\{10\bar{1}2\}$ tensile twins nucleate and propagate in the parent grains resulting in a fully reoriented grain by 5% strain. (b) Contraction twin formation from the $(\bar{1}102)$ and $(1\bar{1}02)$ twins' interaction with the GB.

To determine the effect of twin nucleation on growth, we measured the GB perimeter fraction at which each twin variant nucleated with respect to the overall GB

length. Figure 3.2b shows a plot of this tendency which outlines a noticeable advantage of the $(10\bar{1}2)$ variant. Coupled with twin-twin interactions between the $(01\bar{1}2)$ and $(\bar{1}102)$ variant pairs (green and yellow), stunting twin growth, enhanced nucleation at the GB allowed the $(10\bar{1}2)$ variant pair (red) to dominate overall twinning in AOI 1. By 5% strain, 97.3% of the parent grain has twinned. The twin variant area fractions are plotted in Figure 3.3. The purple grain which was added to AOI 1, shows tension twins detwinning after 1% strain and then proceeds to nucleate contraction twins by 3%. The twins are found to be of the $\{10\bar{1}1\}$ twin family and have a misorientation of 56° (± 8°) (Figure 3.1).

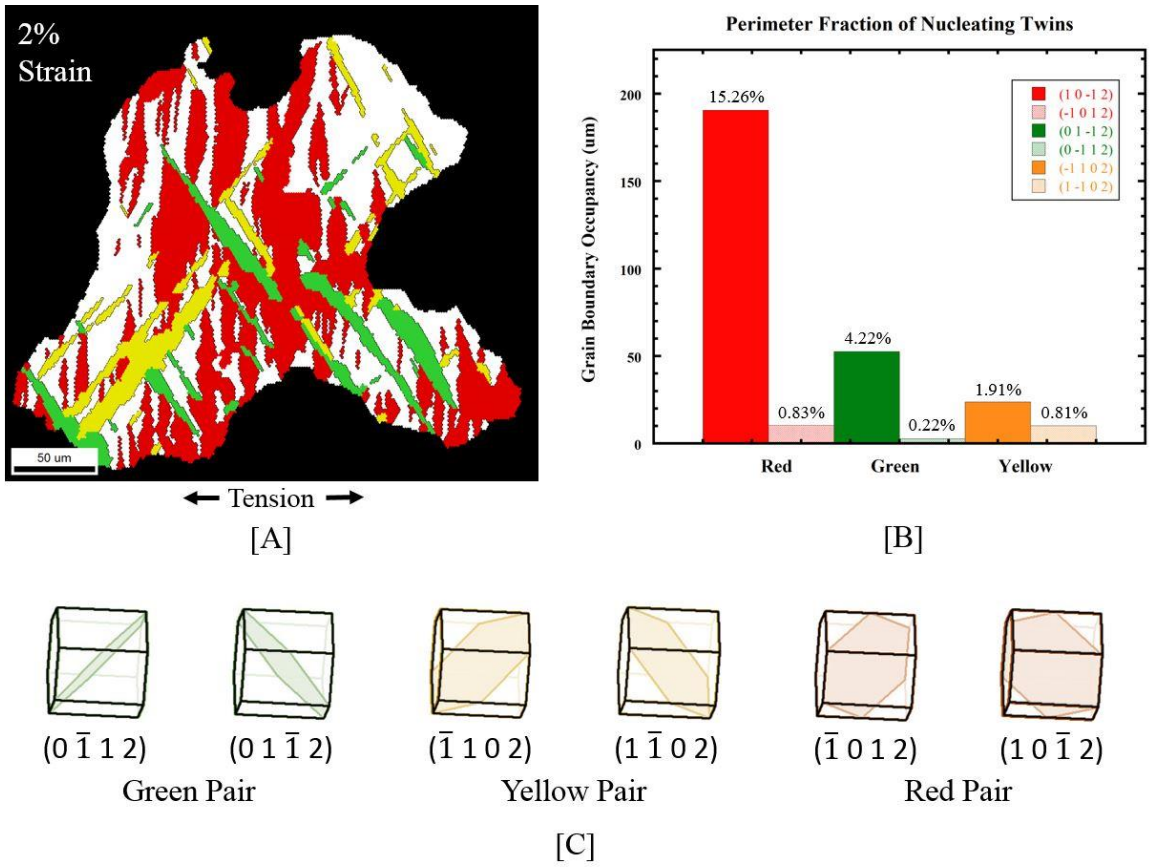

Figure 3.2 Twin variant selection in AOI 1. (a) The orientation map of the three evident twin pairs highlighted in green yellow red. (b) By mapping the grain boundary occupancy of twins at 1% strain (just after nucleation), the perimeter fraction of twinning can be determined. The perimeter fraction shows a clear dominance of $(10\bar{1}2)$ twinning with evident dominate variants within the green and yellow pairs, i.e. $(01\bar{1}2)$ and $(\bar{1}102)$ respectively. (c) The proposed variant pair twin planes are shown within parent orientation with their respective highlighted colors.

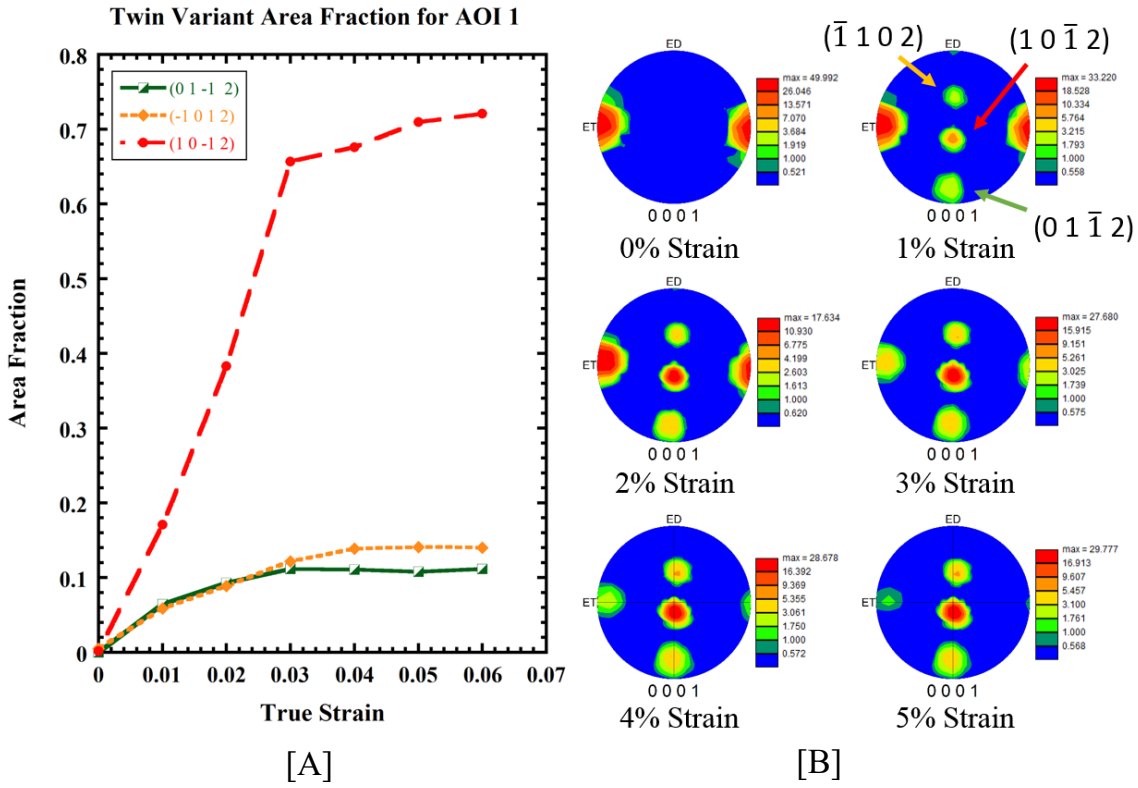

Figure 3.3 (a) Evolution of twin variant area fraction with strain for the three distinct pairs of the $\{10\bar{1}2\}$ system in AOI 1. (b) (0001) pole figures showing the nucleation of three dominate twin variants forming at 1% strain then growing in intensity as the parent orientation diminishes.

The active tensile twins are composed of three distinct pairs. In Figure 3.2a, the tensile twin variants are highlighted in pairs with the respective colors of green, yellow, red, and further crystallographically determined in Figure 3.2c. This maps the twins by their orientation relative to each other instead of a global orientation given by the inverse pole figure. By doing so, all variants are easily distinguished at each strain level without confusing between new nuclei and twin thickening. Figure 3.2b plots each of the variants' nucleation occupancy in the GB at 1% strain. It is important to note that as soon as the strain reached 1%, nucleation nearly ceased and twin fraction dominantly increased by twin thickening. Therefore, the $(10\bar{1}2)$ variant occupies the majority of GB restricting

growth of the $(01\bar{1}2)$ and $(\bar{1}012)$ twin variants. In fact, so few of the recessive variants occupy the GB, their growth is nearly negligible and mostly relies on forming from other twin boundaries.

Even though the $(10\bar{1}2)$ variant pair had a much lower Schmid factor compared to the $(\bar{1}102)$ variant pair, the red variant continued to engulf the parent grain while the yellow variant grew very little after nucleation. This is thought to be an effect of twin-twin interactions between the $(\bar{1}102)$ and $(0\bar{1}12)$ variants as they had competing twin planes. The $(10\bar{1}2)$ variant pair propagated vertically creating less harsh angles of interactions between neighboring twins.

3.2 The Characterization of Contraction Twinning in AOI 2

The second area of interest has a very different orientation compared to AOI 1. AOI 2 is composed of the three primary grains with a basal orientation (0001). This orientation belongs to the weak texture of the double-fiber. The basal orientation aligns the c-axis perpendicular to the loading direction, which leads to contraction of the c-axis.

$\{10\bar{1}1\}$ twinning and shear bands formed from contraction twins, have been noted for failure in plane-strain compression [26]. $\{10\bar{1}1\}$ contraction twins usually remain as thin and needle-like lamellae, fact that was attributed to the low mobility of twinning disconnections due to the step height and the complexity of atomic shuffling requirements [27]. The formation of $\{10\bar{1}1\}$ twins is believed to occur at relatively high stress levels due to their very large critical resolved shear stress (CRSS) [20]. Although contraction twins formed from a compressive and tensile load are exactly of the same crystallographic nature, $\{10\bar{1}1\}[10\bar{1}2]$, contraction twins in this tensile study have been

observed to nucleate at substantially lower CRSS, well below previously reported values in the literature when the c-axis was under plain strain compression.

The progression of damage in AOI 2 is shown in Figure 3.4a and surprisingly thin needle-like structures are nucleating at strains as low as 2%. At 0% strain, a tensile twin has formed likely due to handling of the specimen as the twin detwins with increasing strain. By 2% strain, contraction twins with SF of 0.209 and 0.448 have formed, while there is evidence of another about to nucleate. By 5% strain, multiple contraction twins are formed, and large distortions can be observed within the parent grain. Like tensile twins, contraction twins are characterized based on their misorientation with the parent along the boundary (56°).

Like AOI 1, the SF of possible slip systems as well as the $\{10\bar{1}1\}$ contraction twins are compared in Table 3.3. When comparing these values, contraction twins are not likely to contribute significantly to the deformation accommodation as prismatic and pyramidal slip modes.

In an effort to understand the reason for $\{\bar{1}011\}$ twin to nucleate at lower stress level in tension than in compressive stress states with respect to the c-axis stress sign, we performed more detailed characterization of their micro texture and microstructural conditions within AOI 2. Figure 3.5 displays the highlighted contraction twins that are grouped by $\{10\bar{1}1\}$ distinct pairs. For this characterization the $(\bar{1}101)$ pair is blue, $(0\bar{1}11)$ pair is green, and the $(\bar{1}011)$ pair is orange. The selection of the pairs were determined by relating the actual orientation of the twins (Pole Figure in Figure 3.5b) to the idealized orientation of $\{10\bar{1}1\}$ contraction twins (Pole Figure in Figure 3.5c). As

expected, the actual orientations do not precisely relate to the idealized orientation but the general orientations match with reasonable accuracy.

However, by 4% strain, the contraction twins have begun to experience twinning in their lattice, a phenomenon known as double twinning or retwinning. This process has been characterized at length in early literature [16,28–32]. Double twinning occurs when a residual twin accommodates the increasing strain by retwinning its own lattice. This process is common to an extension twin in which a compression twin nucleates [17]. The misorientation of the parent grain is not 86°, as with most tensile twins, but instead 38° ± 7° of $(1\bar{2}10)$ [19]. In Figure 3.6, all of the boundaries meeting the prescribed misorientations are highlighted in black.

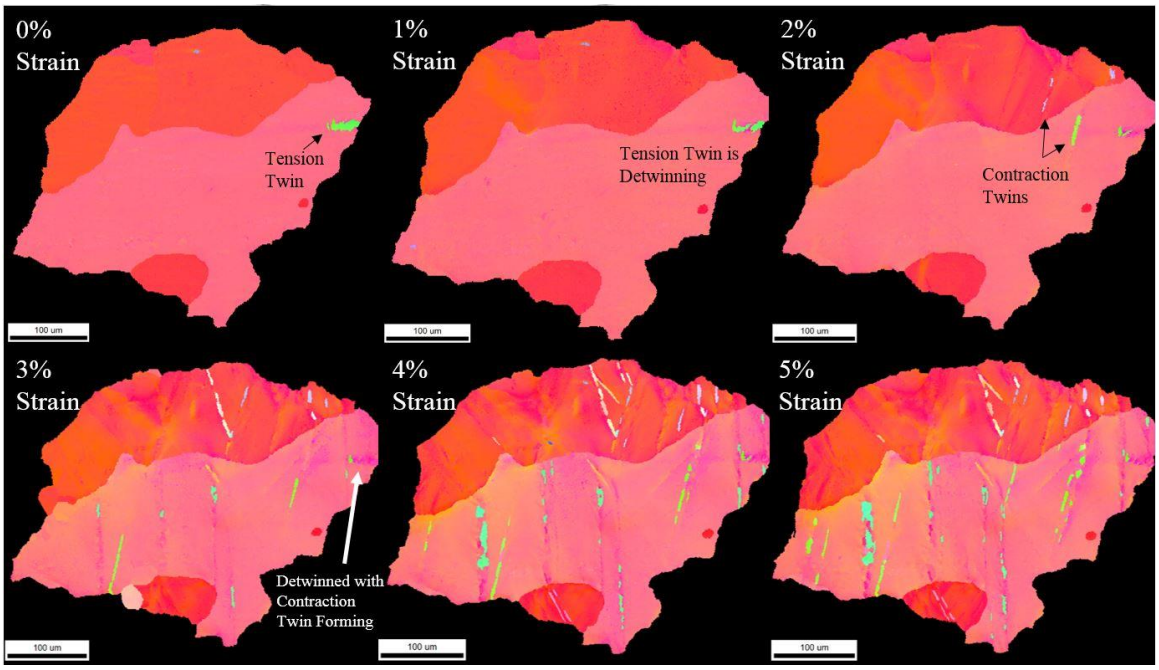

[A]

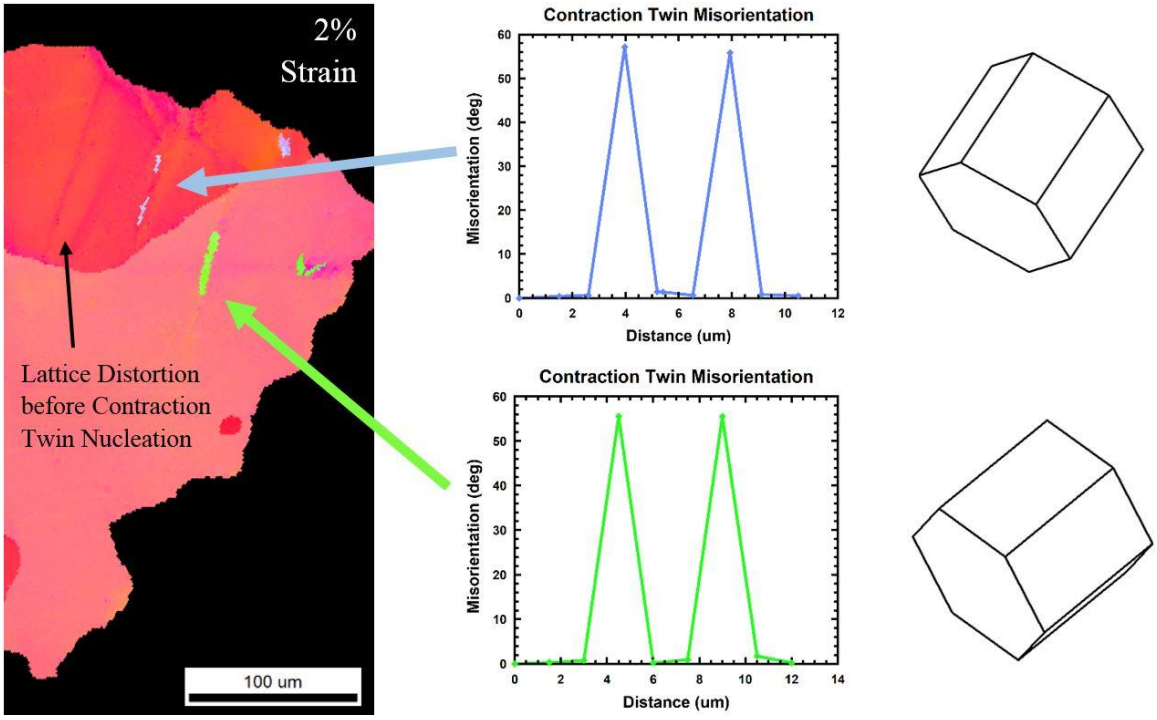

[B]

Figure 3.4 (a) Inverse pole maps revealing lattice reorientation due to profuse nucleation of $\{10\bar{1}1\}$ contraction twinning and slip as deformation proceeds from 0% to 5%. Although pyramidal slip ⟨c+a⟩ has a relatively

higher SF, there is profuse nucleation of contraction twins. (b) The misorientation data of the twins indicates the presence of contraction twins as early as 2% of strain with unit crystal orientation of both twins.

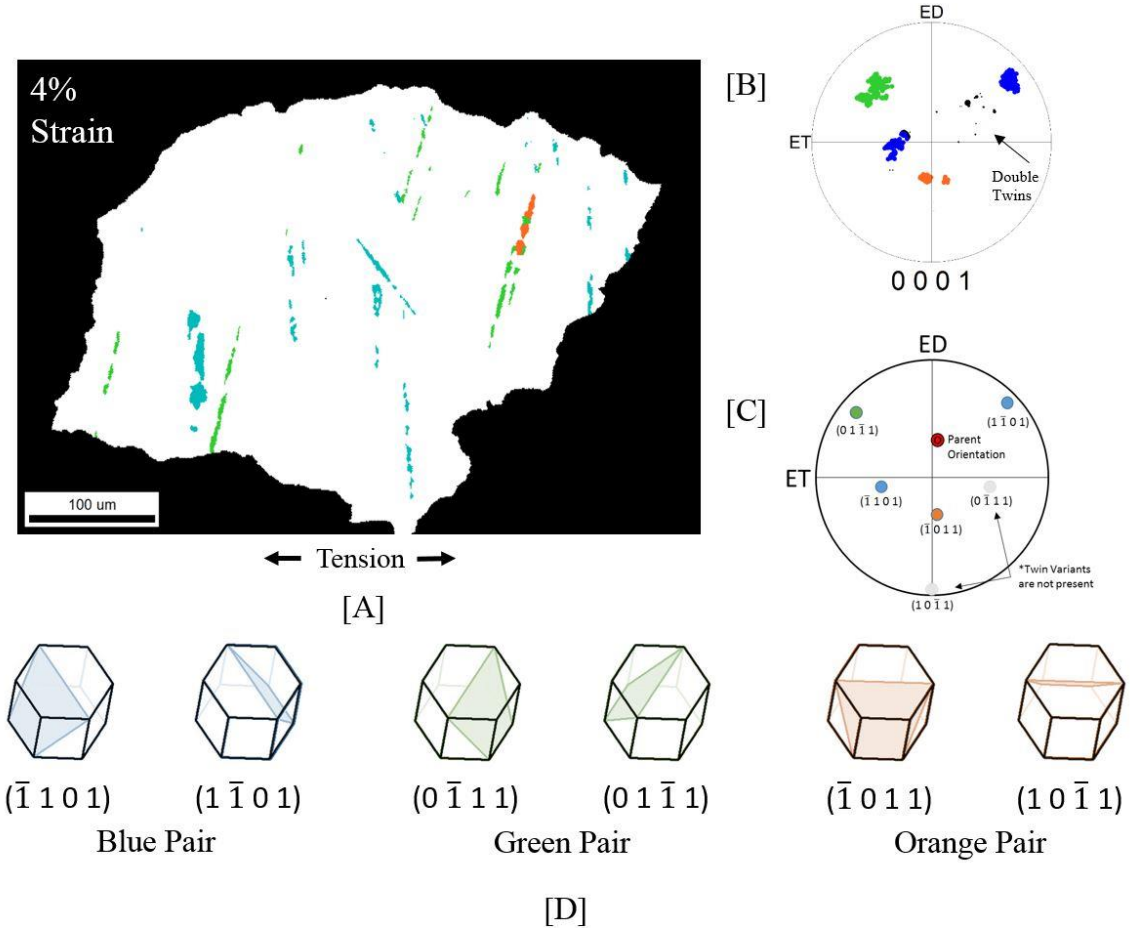

Figure 3.5 Characterization of $\{10\bar{1}1\}$ contraction twins at (a) 4% strain revealing continuous nucleation of new twin variants. The twins were individually selected to be partitioned from the parent grain. The texture of the partitioned twins is shown in part (b). Double twins are found among the partitioned twins. The idealized texture of $\{10\bar{1}1\}$ contraction twins is shown in part (c). Not all twin variants are present, but they are representatives of each twin pair are. The contraction twin variants are characterized by their respective color pair highlighted in the parent grain (a), PF (b, c), and crystal lattice (d).

To verify the presence of double twinning, a twin of the $(01\bar{1}1)$ green pair was selected at 3% strain (Figure 3.6). This twin has completed its growth by 3% strain and shows evidence of double twinning by 4% of strain, which creates an attractive location

for further analysis. The misorientation data shows that the twin is indeed a contraction twin at 3% strain and then twins again by 4% strain making a misorientation with the parent grain of 36°. It looks like the contraction twin reorients the lattice to a very favorable orientation for tension twinning which enjoys a very low critical resolved shear stress, prompting the double twinning effect. This event leads to an interface where perhaps neither of the tension or contraction glissile twinning disconnection can glide, and thus stopping the thickening of the twin lamella. This double twinning phenomenon clearly explains the thin-needle shape of contraction twins, as tension twinning and a modification of the interface atomic structure rapidly plague them.

Table 3.3 Values of Resolved Shear Stress and Schmid factors determined by a $[2\bar{1}\bar{1}0]$ loading with applied stress at 2% Strain of ET-Tension in Figure 2.2

	Slip or Twin Plane (h k (i) l) [u v (t) w]	Schmid Factor m	Resolved Shear Stress RSS (MPa)
Tension Twin Variants	$(\bar{1}\ 0\ 1\ 1)\ [1\ 0\ \bar{1}\ 2]$	-0.311	21.77
	$(1\ 0\ \bar{1}\ 1)\ [\bar{1}\ 0\ 1\ 2]$	-0.311	21.77
	$(0\ \bar{1}\ 1\ 1)\ [0\ 1\ \bar{1}\ 2]$	0	-
	$(0\ 1\ \bar{1}\ 1)\ [0\ \bar{1}\ 1\ 2]$	0	-
	$(1\ \bar{1}\ 0\ 1)\ [\bar{1}\ 1\ 0\ 2]$	-0.311	21.77
	$(\bar{1}\ 1\ 0\ 1)\ [1\ \bar{1}\ 0\ 2]$	-0.311	21.77
Slip Systems	Basal $\langle a \rangle$	0	-
	Prismatic $\langle a \rangle$	0.433	30.31
	Pyramidal $\langle a \rangle$	0.382	26.74
	Pyramidal $\langle c + a \rangle$	0.446	31.22

Nonetheless, the reason why $\{10\bar{1}1\}$ twinning is easier to nucleate in tension than in compression will be difficult to explain or prove. This CRSS dependence on stress sign for twinning could however be addressed from the following perspective. It is known that twinning in hcp metals require both atomic movement by both shear and shuffle. El Kadiri et al. [26] advanced a theory which provides analytical solutions for the vector displacements for both shear and shuffle for any compound twin. Schmid effects are associated with accommodations through shear, which is the most fundamental and unquestionable condition for dislocation and disconnection motion. However, shuffles can be viewed as atomic movement due to diffusion. In general, the only component of stress that drives diffusion is the hydrostatic pressure or more precisely gradient of hydrostatic pressure. As shuffle is a pure diffusion phenomenon, it could be readily sensitive to the local state of hydrostatic pressure in the disconnection core as its glide along the twin interface. That is, the inherent difference in the stress state between tension and compression could have profound implications on the ease of shuffle and does the mobility of disconnections. As such, one can hypothesize that a complex stress state is acting on the c-axis of the unit crystal lattice aiding the shuffle associated with twin formation thereby reducing the required stress to induce shear through twinning or slip (Figure 3.7).

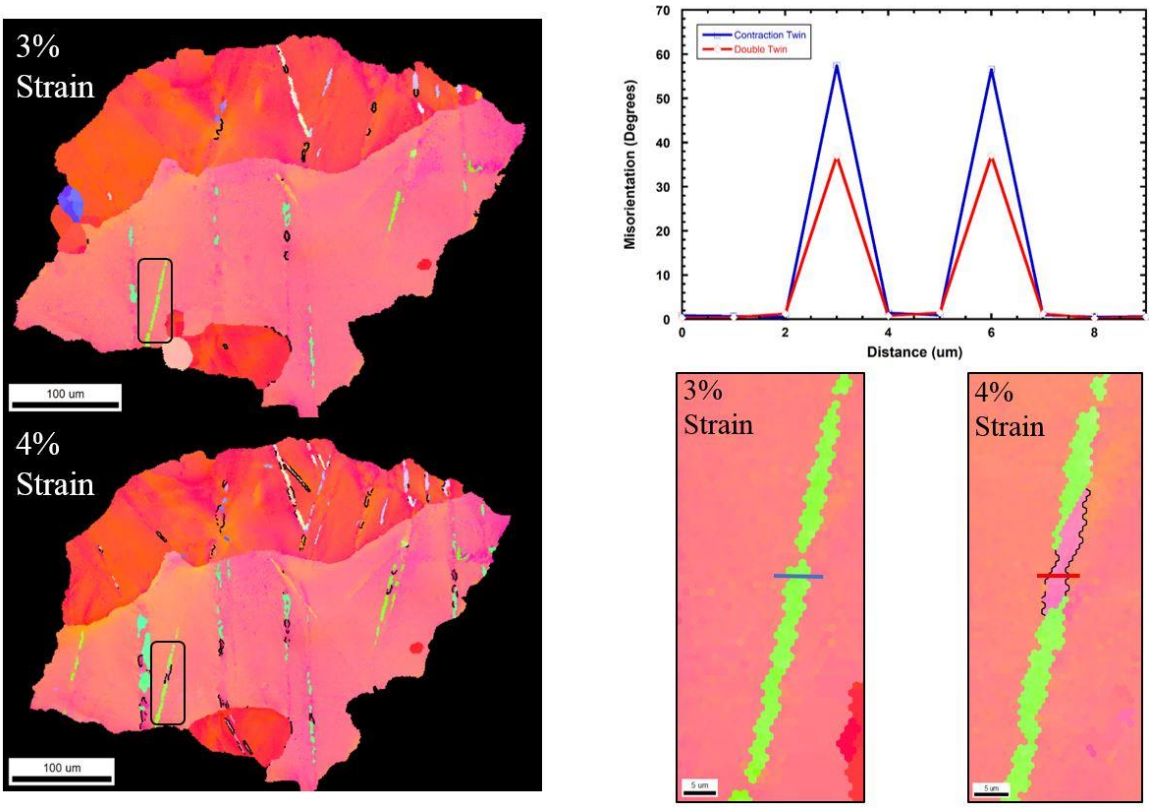

Figure 3.6 Characterization of double twinning at low stresses. The twin of interest is fully formed by 3% strain and does not show signs of double twinning. By 4% strain, the twin of interest begins to double twin at the middle. Misorientation analysis between the double twin and the contraction twin is compared to confirm the presence of contraction and double twins.

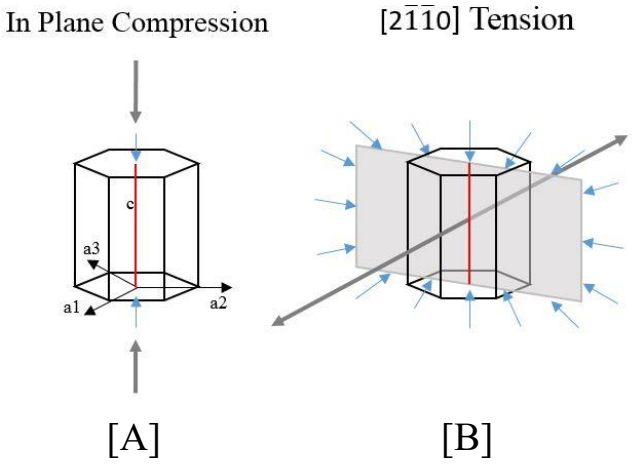

Figure 3.7 Comparison of the stress states experienced by (a) In Plane Compression and (b) [$2\bar{1}\bar{1}0$] Tension. The representation of [$2\bar{1}\bar{1}0$] Tension is simplified

to a two-dimensional planer stress representing the plane of maximum compression in an attempt to visualize the complexity of the stress state experienced by contraction of the c-axis due to Poisson Effects.

3.3 Twin-interactions Induced Cracks

Coupled EBSD and FEG-SEM micrographic characterization at different strain levels revealed cracks nucleating at the intersection between two intersecting $\{10\bar{1}2\}$ twins, slip bands, grain boundaries. Figures 3.8-3.10, gathered by Bratton [33], depict tension twin interactions with slip, GB and other twins, respectively. In all these cases the SF for the twins implicated in damage was low and their growth was slow.

For the case of slip-twin interaction (Figure 3.8), one possible mechanism is the difficulty for the twin to facet or form a disconnection as a dislocation rams into the interface [34–38]. This will lead to an accumulation of dislocations and potential slip bands that promote strain incompatibility and hots spots inside the twin domains. These phenomena could be exacerbated by the transmutation effect which would increase the density of sessile dislocations.

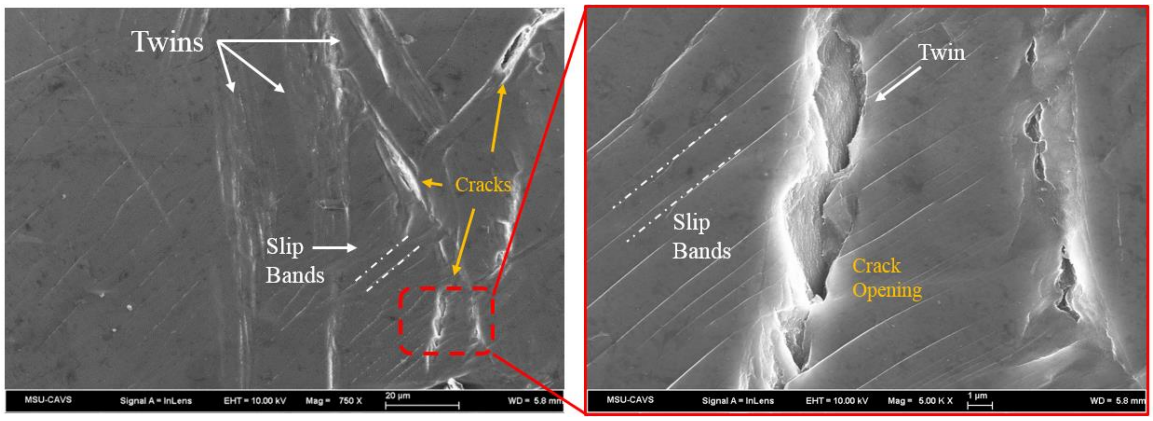

Figure 3.8 Micrographs depicting Slip-Twin interactions' involvement in crack nucleation [33]

For the case of cracks nucleating at the twin-GB intersections, one plausible explanation is the difficulty to accommodate strain at the GB due to the unfavorable orientation of the next grain to accommodate the local stress by easy slip. Propagating twins move through the grain until they reach the boundary at which the stress ahead of the twin must be accommodated. In the case of a grain orientation favorable for twinning, typical case of sharp textures, a new twin is formed giving rise to autocatalytic twinning. However, if the orientation requires activation of hard slip, a crack may nucleate.

For the case of cracks nucleating at twin-twin intersections, interactions between opposing twins have shown detrimental effects on hardening which leads to fracture [14,15,39–41]. When an incident twin encounters an obstacle twin, the strain can be accommodated in the following manners: retwinning of the obstacle twin, slip in the incident or obstacle twin, and detwinning of the incident twin [6,39,42]. As described by Beyerlein and Tomé [43], grains with multivariant twinning are more likely to rapidly strain harden due to the fact of lower CRSS of twin propagation compared to nucleation and have been associated with fracture in literature since 1957 by Reed-Hill [5,44,45] or even sooner. Twins similar to the green and yellow variants found in AOI 1, impede the variants growth building strain until a crack nucleates (Figure 3.10). This phenomenon might be exacerbated in the case of low SF twins, as their lack of thickening might promote strong strain incompatibilities at the triple junction and likelihood of debonding between the two twins.

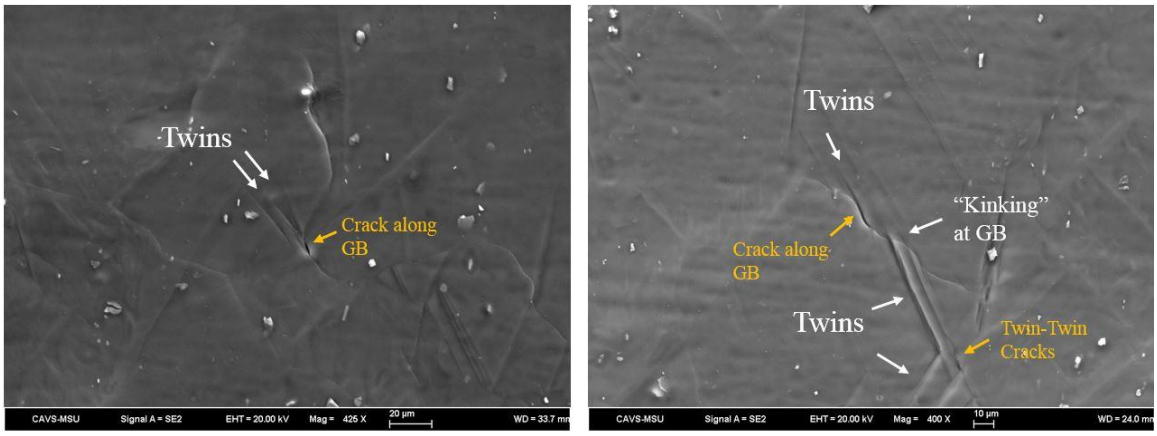

[A] [B]

Figure 3.9 Twin-GB interactions lead to crack nucleation (a) due to a lack of strain accommodation. (b) Proper accommodation of strain is found at the surface where GB emerges through "kinking." However, a crack is formed at the GB from interactions with another twin. Cracks are also noted from twin-twin interactions [33].

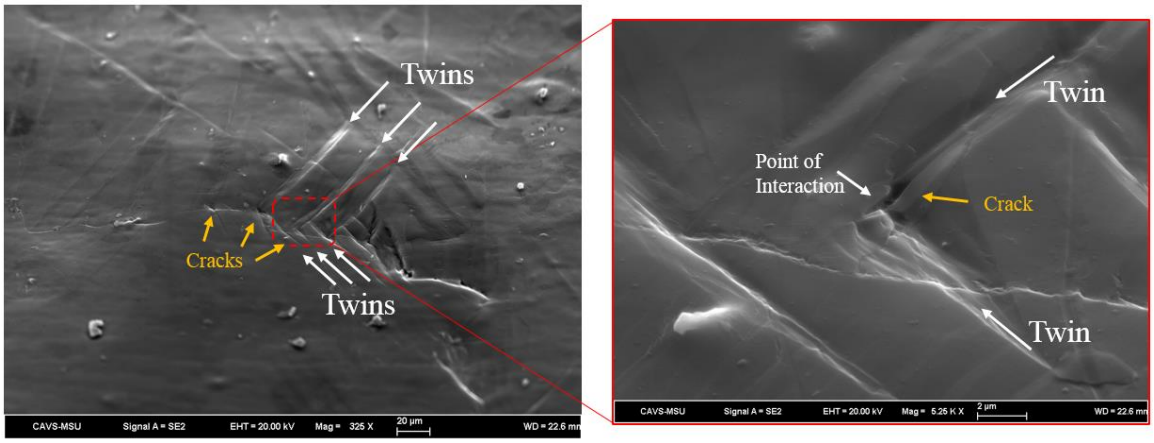

Figure 3.10 Micrographs of $\{10\bar{1}2\}$ Twin-Twin interactions and their involvement in crack nucleation [33].

Double twinning has been used to describe multifold twinning within an original twin since the 1960's [46]. Within Mg, double twinning enhances damage and commonly occurs with $\{10\bar{1}1\}$ twins forming within a $\{10\bar{1}2\}$ tensile twin [16,17,19,47–51]. However, in the case of this study, contraction twins are found forming at relatively low

stresses and are not formed through double twinning. As discussed before, contraction twins are to be considered a distinct twinning mode due to the complex mixed stress state experienced by crystal lattice. In fact, due to the orientation of contraction twins, cracks nucleate sooner and more abruptly. This is evident in the massive cracks formed in Figures 3.11 and 3.12.

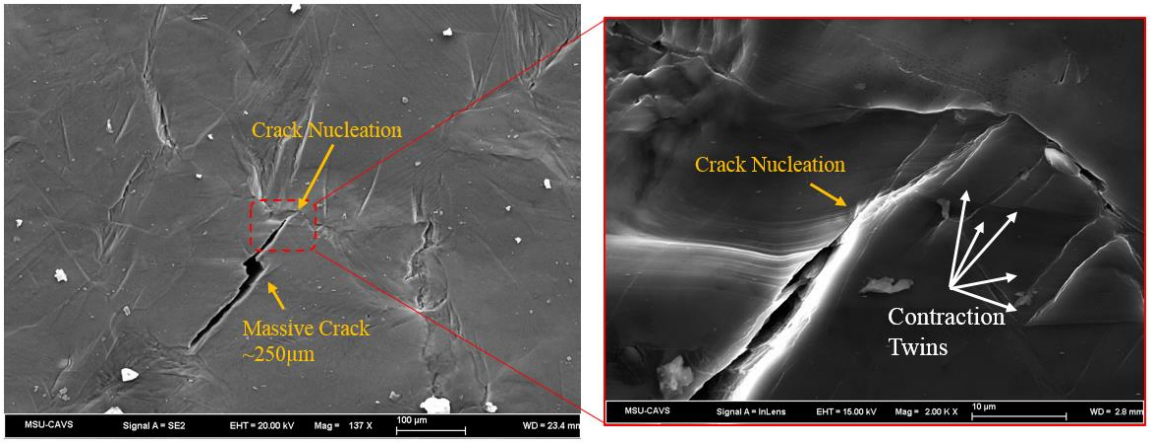

Figure 3.11 Micrographs of evident contraction twins near massive crack nucleation [33].

Notice the contraction twins are located in a parent grain and did not form through double twinning. Figure 3.12 shows the misorientation of the twin with the parent to be 56° and not the 38° of $(1\bar{2}10)$ expected for double twinning [19,49]. In addition, the size and shape are that of a contraction twin, while a double twin would fill the silhouette of the original twin.

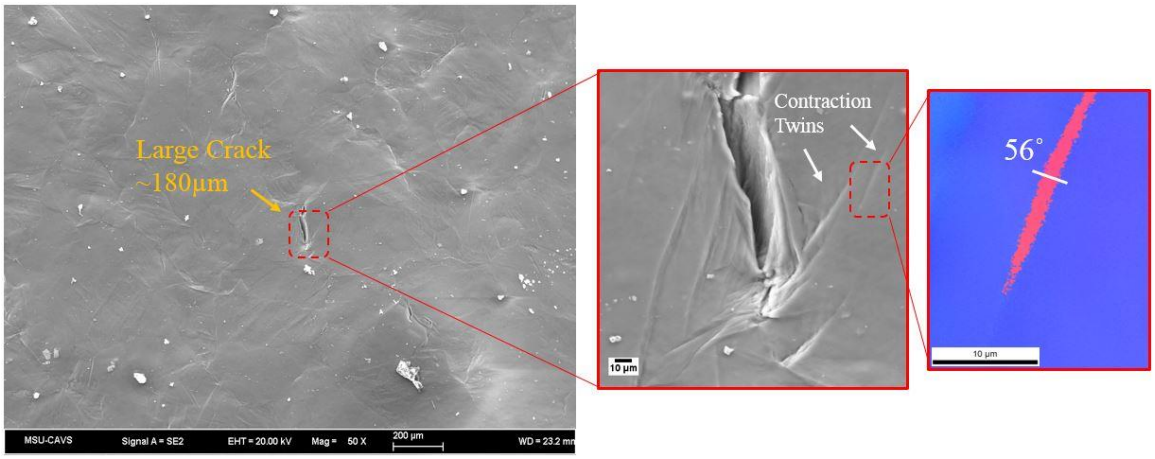

Figure 3.12 Large crack formation due to contraction twin interactions. The contraction twins are found to have a misorientation of 56° [33].

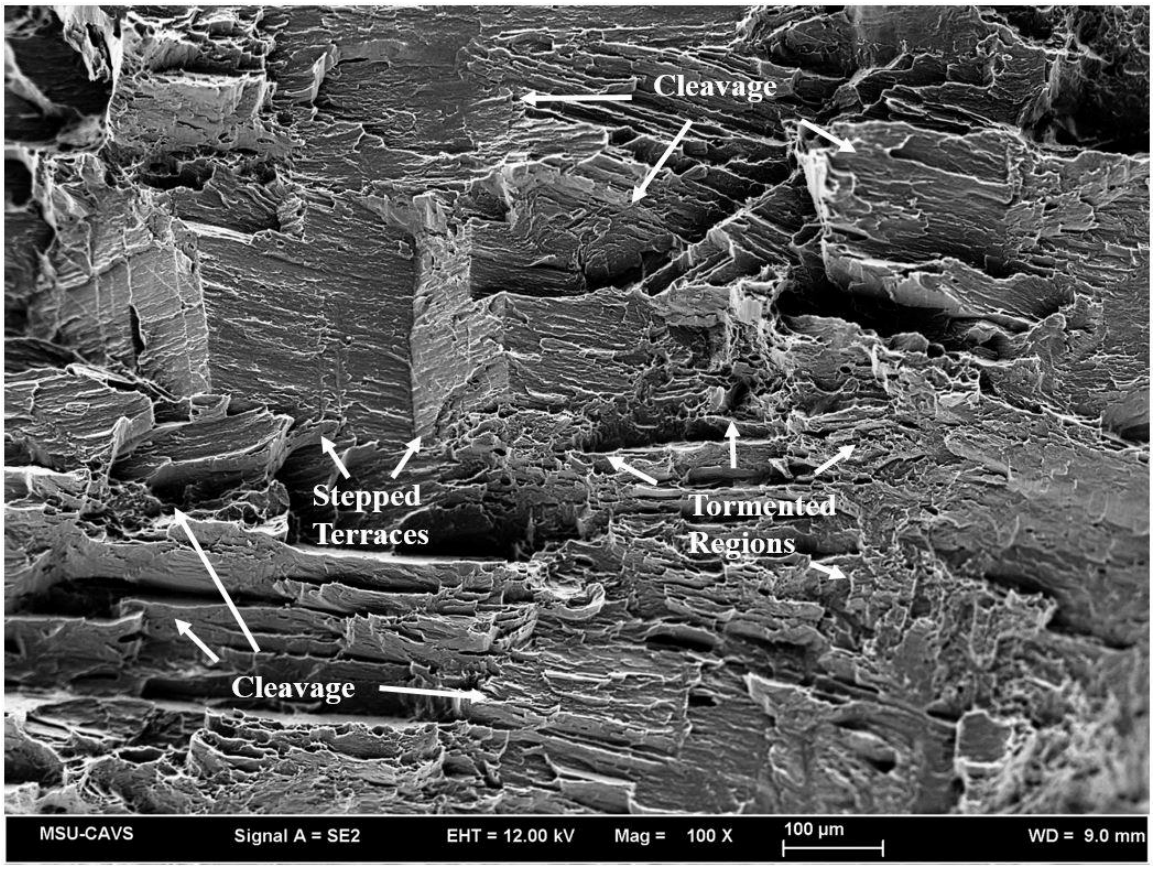

Figure 3.13 Micrograph shows evidence of dual phase fracture. Cleavage and stepped terraces formed from twin interactions caused brittle failure while the tormented regions induced ductile failure [33].

Contraction twin induced damage could be explained by the inability of slip to penetrate the hard contraction twin boundary, creating large areas of cleavage and stepped terraces within the fracture surface commonly related to brittle failure (Figure 3.13). The tormented areas are caused by slip deformation around the twin and grain boundaries and are commonly related to ductile failure.

CHAPTER IV

CONCLUSIONS

To summarize this work, a multistage chart is schematized to outline the impact of the fundamental mechanisms driving damage in magnesium alloys (Figure 4.1). The double-fiber texture generated by the extrusion of the magnesium AM30 hollow tube rail, allowed revealing key features related multivariant twinning under tension, effect of GBs on twin nucleation, and how GB and twin interfaces could contribute to damage. Particularly, a non-Schmid effect was revealed with respect to the greater ease for $\{10\bar{1}1\}$ contraction twins to nucleate under tension than in compression. Damage primarily occurred as a result of interactions of low Schmid factor twins with slip, GBs, and other twins. Furthermore, the ease of twin nucleation at grain boundaries is the primary cause for any difference observed between the volume fractions of different twin variants active in the same grain.

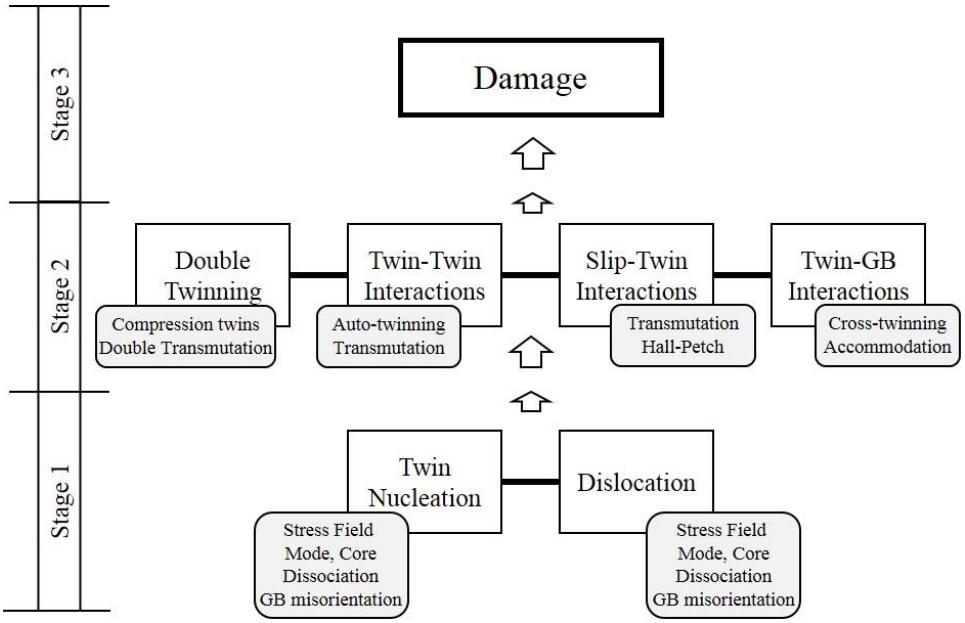

Figure 4.1 Multiscale effects driving plasticity and damage in magnesium.

REFERENCES

[1] P.L. Pratt, S.F. Pugh, Twin accommodation in zinc, J. Inst. Met. 80 (1952) 653–658.

[2] J.J. Gilman, Mechanism of ortho kink-band formation in Compressed Zinc Monocrystals, JOM. 6 (1954) 621–629. doi:10.1007/BF03398884.

[3] H.S. Rosenbaum, Non-basal slip and twin accommodation in zinc crystals, Acta Metall. 9 (1961) 742–748. doi:10.1016/0001-6160(61)90104-3.

[4] H.S. Rosenbaum, Deformation twinning, Gordon Breach N. Y. 43 (1964).

[5] R.E. Reed-Hill, Twin intersections & Cahns Continuity Conditions, Trans. Metall. Soc. AIME. 230 (1964) 809.

[6] A.W. Sleeswyk, Emissary dislocations: Theory and experiments on the propagation of deformation twins in α-iron, Acta Metall. 10 (1962) 705–725. doi:10.1016/0001-6160(62)90040-8.

[7] A.W. Sleeswyk, Twinning and the origin of cleavage nuclei in α-iron, Acta Metall. 10 (1962) 803–812. doi:10.1016/0001-6160(62)90094-9.

[8] A.W. Sleeswyk, ½<111> screw dislocations and the nucleation of {112}<111> twins in the b.c.c. lattice: The Philosophical Magazine: A Journal of Theoretical Experimental and Applied Physics: Vol 8, No 93, (1963). https://www.tandfonline.com/doi/abs/10.1080/14786436308207311.

[9] M.R. Barnett, N. Stanford, P. Cizek, A. Beer, Z. Xuebin, Z. Keshavarz, Deformation mechanisms in Mg alloys and the challenge of extending room-temperature plasticity, JOM. 61 (2009) 19–24. doi:10.1007/s11837-009-0115-6.

[10] Y. Zhang, P.C. Millett, M. Tonks, B. Biner, Deformation-twin-induced grain boundary failure, Scr. Mater. (2011). doi:10.1016/j.scriptamat.2011.10.021.

[11] J. Holden, XCVII. Plastic deformation features on cleavage surfaces of metal crystals, Lond. Edinb. Dublin Philos. Mag. J. Sci. 43 (1952) 976–984. doi:10.1080/14786440908521009.

[12] F.J. Zerilli, R.W. Armstrong, Constitutive relations for the plastic deformation of metals, AIP Conf. Proc. 309 (1994) 989–992. doi:10.1063/1.46201.

[13] F.J. Zerilli, R.W. Armstrong, Dislocation Mechanics Based analysis of Material Dynamics Behavior : Enhanced Ductility, Deformation Twinning, Shock Deformation, Shear Instability, Dynamic Recovery, J. Phys. IV. 07 (1997) C3-637-C3-642. doi:10.1051/jp4:19973109.

[14] L. Rémy, The interaction between slip and twinning systems and the influence of twinning on the mechanical behavior of fcc metals and alloys, Metall. Trans. A. 12 (1981) 387–408. doi:10.1007/BF02648536.

[15] L. Rémy, Twin-slip interaction in f.c.c. crystals, Acta Metall. 25 (1977) 711–714. doi:10.1016/0001-6160(77)90013-X.

[16] Q. Ma, H. El Kadiri, A.L. Oppedal, J.C. Baird, M.F. Horstemeyer, M. Cherkaoui, Twinning and double twinning upon compression of prismatic textures in an AM30 magnesium alloy, Scr. Mater. 64 (2011) 813–816. doi:10.1016/j.scriptamat.2011.01.003.

[17] Q. Ma, H. El Kadiri, A.L. Oppedal, J.C. Baird, B. Li, M.F. Horstemeyer, S.C. Vogel, Twinning effects in a rod-textured AM30 Magnesium alloy, Int. J. Plast. 29 (2012) 60–76. doi:10.1016/j.ijplas.2011.08.001.

[18] M.R. Barnett, Twinning and the ductility of magnesium alloys: Part I: “Tension” twins, Mater. Sci. Eng. A. 464 (2007) 1–7. doi:10.1016/j.msea.2006.12.037.

[19] M.R. Barnett, Twinning and the ductility of magnesium alloys: Part II. “Contraction” twins, Mater. Sci. Eng. A. 464 (2007) 8–16. doi:10.1016/j.msea.2007.02.109.

[20] A.L. Oppedal, H. El Kadiri, C.N. Tomé, G.C. Kaschner, S.C. Vogel, J.C. Baird, M.F. Horstemeyer, Effect of dislocation transmutation on modeling hardening mechanisms by twinning in magnesium, Int. J. Plast. 30–31 (2012) 41–61. doi:10.1016/j.ijplas.2011.09.002.

[21] H. El Kadiri, J.C. Baird, J. Kapil, A.L. Oppedal, M. Cherkaoui, S.C. Vogel, Flow asymmetry and nucleation stresses of {101¯2} twinning and non-basal slip in magnesium, Int. J. Plast. 44 (2013) 111–120. doi:10.1016/j.ijplas.2012.11.004.

[22] H.-R. Wenk, L. Lutterotti, S. Vogel, Texture analysis with the new HIPPO TOF diffractometer, Nucl. Instrum. Methods Phys. Res. Sect. Accel. Spectrometers Detect. Assoc. Equip. 515 (2003) 575–588. doi:10.1016/j.nima.2003.05.001.

[23] H.-R. Wenk, L. Lutterotti, S.C. Vogel, Rietveld texture analysis from TOF neutron diffraction data, Powder Diffr. 25 (2010) 283–296. doi:10.1154/1.3479004.

[24] R. Hielscher, H. Schaeben, A novel pole figure inversion method: specification of the MTEX algorithm, J. Appl. Crystallogr. 41 (2008) 1024–1037. doi:10.1107/S0021889808030112.

[25] E. Schmid, W. Boas, Plasticity of crystals, (1935).

[26] E.W. Kelley, W. Hosford, Plane-strain compression of magnesium and magnesium alloy crystals, Trans Met Soc AIME. 242 (1968) 5–13.

[27] H. El Kadiri, C.D. Barrett, M.A. Tschopp, The candidacy of shuffle and shear during compound twinning in hexagonal close-packed structures, Acta Mater. 61 (2013) 7646–7659. doi:10.1016/j.actamat.2013.09.002.

[28] Z. Keshavarz, M.R. Barnett, EBSD analysis of deformation modes in Mg–3Al–1Zn, Scr. Mater. 55 (2006) 915–918. doi:10.1016/j.scriptamat.2006.07.036.

[29] S.W. Xu, S. Kamado, N. Matsumoto, T. Honma, Y. Kojima, Recrystallization mechanism of as-cast AZ91 magnesium alloy during hot compressive deformation, Mater. Sci. Eng. A. 527 (2009) 52–60. doi:10.1016/j.msea.2009.08.062.

[30] M.R. Barnett, Z. Keshavarz, A.G. Beer, X. Ma, Non-Schmid behaviour during secondary twinning in a polycrystalline magnesium alloy, Acta Mater. 56 (2008) 5–15. doi:10.1016/j.actamat.2007.08.034.

[31] T. Al-Samman, G. Gottstein, Room temperature formability of a magnesium AZ31 alloy: Examining the role of texture on the deformation mechanisms, Mater. Sci. Eng. A. 488 (2008) 406–414. doi:10.1016/j.msea.2007.11.056.

[32] I.J. Beyerlein, J. Wang, M.R. Barnett, C.N. Tomé, Double twinning mechanisms in magnesium alloys via dissociation of lattice dislocations, Proc R Soc A. 468 (2012) 1496–1520. doi:10.1098/rspa.2011.0731.

[33] N.R. Bratton, The role of twinning in the initiation of fracture in AM30 and AZ61 magnesium alloys. [electronic resoource], Mississippi State : Mississippi State University, 2012., 2012.

[34] C.D. Barrett, H. El Kadiri, M.A. Tschopp, Breakdown of the Schmid law in homogeneous and heterogeneous nucleation events of slip and twinning in magnesium, J. Mech. Phys. Solids. 60 (2012) 2084–2099. doi:10.1016/j.jmps.2012.06.015.

[35] C.D. Barrett, H. El Kadiri, The roles of grain boundary dislocations and disclinations in the nucleation of $\{10\bar{1}2\}$ twinning, Acta Mater. 63 (2014) 1–15. doi:10.1016/j.actamat.2013.09.012.

[36] H. El Kadiri, C.D. Barrett, J. Wang, C.N. Tomé, Why are {101¯2} twins profuse in magnesium?, Acta Mater. 85 (2015) 354–361. doi:10.1016/j.actamat.2014.11.033.

[37] C.D. Barrett, H. El Kadiri, Impact of deformation faceting on {101¯2},{101¯1} and {101¯3} embryonic twin nucleation in hexagonal close-packed metals, Acta Mater. 70 (2014) 137–161. doi:10.1016/j.actamat.2014.02.018.

[38] C.D. Barrett, M.A. Tschopp, H. El Kadiri, Automated analysis of twins in hexagonal close-packed metals using molecular dynamics, Scr. Mater. 66 (2012) 666–669. doi:10.1016/j.scriptamat.2012.01.034.

[39] S. Mahajan, Twin-slip and twin-twin interactions in Mo-35 at. % Re alloy, Philos. Mag. J. Theor. Exp. Appl. Phys. 23 (1971) 781–794. doi:10.1080/14786437108216988.

[40] S. Mahajan, G.Y. Chin, Twin-slip, twin-twin and slip-twin interactions in Co-8 wt.% Fe alloy single crystals, Acta Metall. 21 (1973) 173–179. doi:10.1016/0001-6160(73)90059-X.

[41] S. Mahajan, G.Y. Chin, Formation of deformation twins in f.c.c. crystals, Acta Metall. 21 (1973) 1353–1363. doi:10.1016/0001-6160(73)90085-0.

[42] A.W. Sleeswyk, C.A. Verbraak, Incorporation of slip dislocations in mechanical twins, Acta Metall. 9 (1961) 917–927. doi:10.1016/0001-6160(61)90110-9.

[43] I.J. Beyerlein, C.N. Tomé, A dislocation-based constitutive law for pure Zr including temperature effects, Int. J. Plast. 24 (2008) 867–895. doi:10.1016/j.ijplas.2007.07.017.

[44] R.E. Reed-Hill, W.D. Robertson, The crystallographic characteristics of fracture in magnesium single crystals, Acta Metall. 5 (1957) 728–737. doi:10.1016/0001-6160(57)90075-5.

[45] G.Y. Chin, The inhomogeneity of plastic deformation, RE Reed-Hill ASM Ohio. (1973) 83–112.

[46] A.G. Crocker, Double twinning, Philos. Mag. J. Theor. Exp. Appl. Phys. 7 (1962) 1901–1924. doi:10.1080/14786436208213854.

[47] P. Cizek, M.R. Barnett, Characteristics of the contraction twins formed close to the fracture surface in Mg–3Al–1Zn alloy deformed in tension, Scr. Mater. 59 (2008) 959–962. doi:10.1016/j.scriptamat.2008.06.041.

[48] W.H. Hartt, R.E. Reed-Hill, Internal deformation and fracture of second order 1011-1012 twins in magnesium, (1965). https://ntrs.nasa.gov/search.jsp?R=19680005173.

[49] B.C. Wonsiewicz, Plasticity of magnesium crystals., PhD Thesis, Massachusetts Institute of Technology, 1966.

[50] J. Koike, Enhanced deformation mechanisms by anisotropic plasticity in polycrystalline Mg alloys at room temperature, Metall. Mater. Trans. A. 36 (2005) 1689–1696. doi:10.1007/s11661-005-0032-4.

[51] J. Koike, N. Fujiyama, D. Ando, Y. Sutou, Roles of deformation twinning and dislocation slip in the fatigue failure mechanism of AZ31 Mg alloys, Scr. Mater. 63 (2010) 747–750. doi:10.1016/j.scriptamat.2010.03.021.